

Targeting excessive *MYCN* expression using MLN8237 and JQ1 impairs the growth of hepatoblastoma cells

CORINNA EBERHERR¹, ALEXANDER BECK¹, CHRISTIAN VOKUHL², KRISTINA BECKER¹,
BEATE HÄBERLE¹, DIETRICH VON SCHWEINITZ¹ and ROLAND KAPPLER¹

¹Department of Pediatric Surgery, Dr. von Hauner Children's Hospital, University Hospital, LMU Munich, D-80337 Munich;

²Institute of Paidopathology, Pediatric Tumor Registry, Christian-Albrecht's-University Kiel, D-24105 Kiel, Germany

Received July 13, 2018; Accepted January 23, 2019

DOI: 10.3892/ijo.2019.4741

Abstract. Hepatoblastoma (HB) is the most common liver tumor in children under the age of 3 years worldwide. While many patients achieve good outcomes with surgical resection and conventional chemotherapy, there is still a high-risk population that exhibits a poor treatment response and unfavorable prognosis, which warrants the search for novel treatment options. In recent years, it has become clear that genetic events alone are not sufficient to explain the aggressive phenotype of this embryonal malignancy. Instead, epigenetic modifications and aberrant gene expression seem to be key drivers of HB. In the present study, expression analyses such as reverse transcription-quantitative polymerase chain reaction revealed that the oncogene, *MYCN* proto-oncogene basic-helix-loop-helix transcription factor (*MYCN*) was upregulated in HB and other pediatric liver tumors, due to the transcriptional activity of its antisense transcript *MYCN* opposite strand (*MYCNOS*). Pyrosequencing demonstrated the hypomethylated regions in the promoter of *MYCN* and *MYCNOS*, suggesting that an epigenetic mechanism may underlie the induction of aberrant expression. Transient *MYCN* knockdown in HB cells resulted in growth inhibition over time. In addition, treating HB cells with the *MYCN* inhibitors JQ1 and MLN8237 led to the significant downregulation of *MYCN* either at the mRNA or protein levels, respectively. The underlying mechanism of action of the two inhibitors was revealed to be associated with the induction of dose-dependent growth arrest, by arresting cells at either the G1/G0 or G2 phase. Furthermore, MLN8237 and JQ1 were able to cause spindle disturbances and/or apoptosis in HB cells. The present results suggest that *MYCN* may be a promising biomarker for

HB and a potential therapeutic target in patients with tumors overexpressing *MYCN*.

Introduction

Hepatoblastoma (HB) is the most common type of liver tumor in children worldwide and mainly affects infants and toddlers between the ages of 6 months and 3 years (1). The characteristically early manifestation of these embryonal tumors suggests that comparatively few genetic alterations are necessary for the formation of a malignant phenotype (2). In fact, systematic analysis of HB by exome sequencing revealed mutations in the β -catenin (*CTNNB1*) gene as the only recurrent alteration, which occurs in approximately two-thirds of all patients (3,4). The oncogenic mutation of *CTNNB1* is known to trigger the pathological activation of the Wnt signaling pathway, which can also occur in *CTNNB1*-wildtype HB via mutations in the genes, adenomatous polyposis coli, axin 1 and axin 2 (5,6). Notably, the activation of mutant *Ctnnb1* in liver progenitor cells has been shown to cause the development of HB in mice by 26 weeks of age (7). However, although Wnt activation has been proven to drive the development of pediatric liver tumors, identification of other molecular mechanisms that are responsible for the manifestation of different histopathological subtypes of HB and more importantly the varying response to chemotherapy and thus the outcome is still warranted (8).

The use of genome-wide expression analysis methods has not only helped to improve our understanding of the molecular mechanisms that drive tumorigenesis but, by identifying subtype-specific changes, fuels the hope of achieving the biomarker-based stratification of tumors, and thereby improve prognosis estimation and risk-adapted therapies (9). A first step in this direction in the field of HB has been the description of a unique gene signature which allows for, based on an expression determination of only 16 genes, the classification of HB into 2 tumor subtypes (10). These subtypes not only reflect the different phases of liver development, but also show a strong prognostic divergence (10). Thus, tumors of the so-called C1 subtype exhibit a higher degree of differentiation with mostly fetal histology and a better prognosis, while the C2 tumors usually have an embryonic differentiation with a poorer prognosis and a higher tumor stage. One of the genes with a significant differential expression between

Correspondence to: Dr. Roland Kappler, Department of Pediatric Surgery, Dr. von Hauner Children's Hospital, University Hospital, LMU Munich, Lindwurmstr. 2a, D-80337 Munich, Germany
E-mail: roland.kappler@med.uni-muenchen.de

Key words: *MYCN* proto-oncogene basic-helix-loop-helix transcription factor, *MYCN* opposite strand, hepatoblastoma, MLN8237, JQ1

C1 and C2 tumor subtypes was MYCN proto-oncogene basic-helix-loop-helix transcription factor (*MYCN*), which maps to 2p24.1, a chromosomal region known to be frequently duplicated in HB (11). Upregulation of *MYCN* expression serves a crucial role in several tumors, such as lung and breast cancer as well as malignancies of neural origin including glioblastoma, medulloblastoma and neuroblastoma (12). In neuroblastoma, transcriptional upregulation is mainly caused by the amplification of the *MYCN* locus (13). *MYCN* encodes a nuclear phosphoprotein that dimerizes with MYC interacting protein X to form a complex that binds to the regulatory regions of MYCN-regulated genes (14). It is generally believed that aberrant *MYCN* expression increases cellular proliferation by inducing cell-cycle progression as well as inhibiting apoptosis (15). Taken together, these findings qualify MYCN as an interesting target for the treatment of HB.

Materials and methods

Patients and tumor cell lines. A total of 61 liver tumor specimens [47 HB, 4 transitional liver cell tumors (TLCT), and 10 pediatric hepatocellular carcinomas (HCC)] were obtained from 61 pediatric patients (32 males, 29 females) undergoing surgical resection in the Department of Pediatric Surgery (University Hospital, LMU Munich, Munich, Germany). The inclusion criteria were that the patients were aged <20 years and had a histologically proven diagnosis of HB, TLCT or HCC. Patients with underlying liver disease were excluded from the study. The clinicopathological features of the patients are presented in Table I. Written informed consent was obtained from each patient or the parents if younger than 12 years and the study protocol was approved by the Ludwig-Maximilians-University Ethics Committee (Munich, Germany; no. 431-11). Furthermore, 3 human HB cell lines were used, including HepT1 (provided by Dr. Torsten Pietsch, Institute of Neuropathology, University of Bonn, Bonn, Germany), HUH6 (Japanese Collection of Research Bioresources, Osaka, Japan) and HepG2 (American Type Culture Collection, Manassas, VA, USA) as well as the hepatocellular carcinoma cell line HUH7 (kindly provided by Dr. Enrico de Toni, Department of Medicine 2, University of Munich, Munich, Germany). Cells were grown at 37°C in RPMI-1640 medium (Gibco; Thermo Fisher Scientific, Inc., Waltham, MA, USA) containing 10% fetal calf serum (FCS; Gibco; Thermo Fisher Scientific, Inc.), 1% antibiotics and glutamine supplement.

Reverse transcription-quantitative polymerase chain reaction (RT-qPCR). RNA extraction and purification of tissues and cells as well as cDNA synthesis were performed as described previously (16). Quantification of gene expression was conducted using TaqMan® Gene expression assays (Applied Biosystems; Thermo Fisher Scientific, Inc.) for *MYCN* (Hs00232074_m1), *MYCNOS* (Hs01040745_m1) and the house-keeping gene TATA-box binding protein (*TBP*; Hs00427620_m1) as well as the TaqMan universal MasterMix II (Applied Biosystems; Thermo Fisher Scientific, Inc.) according to the manufacturer's instructions. Primer sequences are commercially unavailable (Applied Biosystems; Thermo Fisher Scientific, Inc.). RT-qPCR amplifications were conducted in doublets on a Mastercycler

Realplex² instrument (Eppendorf, Hamburg, Germany) and consisted of 2 min uracil-N-glycosylase incubation at 50°C, 10 min DNA polymerase activation at 95°C, and 45 cycles of 15 sec denaturation at 95°C, and primer annealing and extension for 1 min at 60°C. The 2^{-ΔΔC_q} method was used to calculate the relative mRNA expression levels from the means of *MYCN/MYCNOS* and *TBP* (17).

Immunohistochemistry. Frozen tumor tissue sections were embedded in Tissue-Tek Optimal Cutting Temperature compound (Sakura Finetek USA, Inc., Torrance, CA, USA; 5 μm-thick), were fixed for 10 min in ice-cold acetone and endogenous peroxidase activity was quenched using 0.3% hydrogen peroxide in bi-distilled water for 10 min. Following 1 h of blocking with 10% FCS at 37°C, the mouse anti-human N-MYC antibody clone B8.4.B (cat. no. sc-53993; Santa Cruz Biotechnology, Inc., Dallas, TX, USA) diluted to 1:200 in PBS was applied to the sections, which were then incubated overnight at 4°C. Following three washes with PBS, the sections were then covered with one drop of anti-mouse immunoglobulin G (IgG; ImmPRESS HRP reagent kit; Vector Laboratories, Inc.; Maravai LifeSciences, San Diego, CA, USA) and incubated for 30 min at room temperature. Signal detection was conducted using the liquid 3,3'-diaminobenzidine substrate chromogen system (Dako; Agilent Technologies, Inc., Santa Clara, CA, USA) for 30 min at 37°C. Sections were then counterstained with hematoxylin for 5 min at 37°C and mounted with glycerol mounting medium (Dako; Agilent Technologies, Inc.). Consecutive sections of the same tumor tissue were then stained with hematoxylin and eosin without prior immunohistochemical detection and used for histopathological evaluation on an Axioplan light microscope (Zeiss GmbH, Jena, Germany) at a magnification of x100 and x200.

Proliferation assays. Cell proliferation was assessed using 3-(4,5-dimethylthiazol-2-yl)-2,5-diphenyltetrazolium bromide (MTT) assays. Cells (of all cell lines) were seeded at a density of 5-10x10³ cells per well into 96-well plates (NUNC, Langensfeld, Germany) in 100 μl cell culture medium. Following overnight attachment, cells were treated for 48 h at 37°C with various concentrations (1, 10, 100 nM, 1 and 10 μM) of MLN8237 (Alistertib; Axon Medchem, Groningen, Netherlands) and JQ1 (BIOMOL International; Enzo Life Sciences, Inc., Farmingdale, NY, USA) or the solvent DMSO (Merck KGaA). Cell lines were alternatively transfected with 200 nM small interfering (si)-RNA Hs_MYCN_6 FlexiTube siRNA (SI03087518; 5'-CGTGCCGGAGTTGGTAAAGAA-3'; Qiagen GmbH, Hilden, Germany) or 200 nM siGENOME non-targeting siRNA #1 (GE Healthcare Dharmacon, Inc., Lafayette, CO, USA; sequences are commercially unavailable) by electroporation and then directly cultured at a density of 5-10x10³ cells in 96-well plates overnight at 37°C prior to subsequent experimentation.

To assess cell viability, 10 μl MTT (Sigma-Aldrich; Dramstadt, Germany) labeling agent (5 mg/ml in PBS) was added to each well prior to 4 h incubation at 37°C. Media-containing wells without cells were used for background estimation. For cell lysis, 100 μl of the SDS-HCl solution (10% SDS/0.01M HCl) was added to each well. The

Table I. Clinicopathological features of different types of pediatric liver cancers and their association with *MYCN* and *MYCNOS* gene expression.

Category	Patients with pediatric liver cancer, n			P-value	
	HB (n=47)	TLCT (n=4)	HCC (n=10) ^a	<i>MYCN</i>	<i>MYCNOS</i>
Age range (months)	0-56	11-128	92-199	0.8414	0.3881
Metastasis				0.9195	0.5297
No	30	3	7		
Yes	17	1	2		
Vascular invasion				0.4371	0.5526
No	38	3	7		
Yes	9	1	2		
Multifocal growth				0.7421	0.8147
No	35	2	6		
Yes	12	2	2		
Extrahepatic growth				0.8020	0.8270
No	44	4	6		
Yes	3	0	2		
PRETEXT stage				0.7402	0.5787
I	3	0	2		
II	12	2	2		
III	21	1	3		
IV	11	1	0		
Embryonal histology				0.0166	0.0130
No	34	4	n.a.		
Yes	13	0	n.a.		
Outcome				0.2936	0.8646
Alive	40	3	8		
Succumbed	7	1	2		

^aFor 3 HCC patients, only limited clinical data were available so some categories do not present the data of the entire patient cohort. n.a., not applicable; HB, hepatoblastoma; TLCT, transitional liver cell tumor; HCC, hepatocellular carcinoma.

plate was incubated overnight at 37°C. Cell viability was detected by measuring the optical density at a wavelength of 595 nm using the GENios multi scanner microplate reader (Tecan Group, Ltd., Männedorf, Switzerland). Each experiment was performed in duplicate.

Cell screening assay. Morphological changes were detected by means of microscopy once the cells had been treated for 48 h at 37°C with vehicle (DMSO), 10 μM MLN8237 (in HepG2 cells only) or 1.0 μM MLN8237 (in HepT1, HUH6 and HUH7 cells), or 10 μM JQ1 (in HepT1 and HepG2 cells) or 0.5 μM JQ1 (in HUH6 and HUH7 cells) using an inverted Axiovert 40 CFL microscope (Zeiss GmbH) equipped with a Powershot G6 digital device (Canon, Inc., Tokyo, Japan).

Western blot analysis. Cells were seeded at a density of 1x10⁶ per 10 cm cell culture dish. Following overnight attachment, cells were treated for 48 h at 37°C with MLN8237, JQ1 (both at 10 μM for HepT1 and HepG2, and 0.5 μM for HUH6 and HUH7) or DMSO. Once treated, non-adherent and adherent

cells were pooled together in ice-cold lysis buffer [0.5% Triton X-100, 1 mM sodium orthovanadate and cComplete Mini protease inhibitor (Roche Diagnostics, Basel, Switzerland)]. Protein lysates were incubated on ice for 30 min with occasional vortexing. Following centrifugation for 30 min at 4°C and 13,000 x g, protein lysates without cell debris were stored at 4°C until use. The protein concentration was determined by a Bio-Rad Protein Assay (Bio-Rad Laboratories, Inc., Hercules, CA, USA). Proteins (20 μg) were loaded on a 4-12% BIS TRIS NuPage Gel (Novex; Thermo Fisher Scientific, Inc.), separated under reducing conditions and then transferred to a nitrocellulose blotting membrane (GE Healthcare Life Sciences, Little Chalfont, UK). Thereafter, membranes were blocked with PBS/0.1% Tween-20/5% non-fat dry milk overnight at 4°C. Next, antibodies including mouse anti-human N-MYC clone B8.4.B (1:500; cat. no. sc-53993; Santa Cruz Biotechnology, Inc.), rabbit anti-human poly(adenosine diphosphate-ribose) polymerase (PARP; 1:1,000; cat. no. 9542) or rabbit anti-human β-actin (1:2,500; cat. no. 4967S; both Cell Signaling Technology, Inc., Danvers, MA, USA)

were added to the cells overnight at 4°C. For detection, membranes were incubated for 1 h at room temperature with horseradish peroxidase-conjugated polyclonal goat anti-rabbit immunoglobulin secondary antibody (1:2,000; cat. no. PO448; Dako; Agilent Technologies, Inc.). Signals were captured using the enhanced western blotting reagent detection system and Hyperfilm high performance autoradiography films (both GE Healthcare, Chicago, IL, USA).

Apoptosis and cell cycle analysis. Cells (all cell lines) were seeded in 6-well plates and following 24 h, exposed to DMSO, MLN8237 or JQ1 at various concentrations (10 μ M for HepG2, and 1 μ M for HepT1, HUH6 and HUH7) for 48 h at 37°C. Fixation and permeabilization of cells were performed by the dropwise addition of 70% ethanol while vortexing and incubating at -20°C for at least 2 h. Permeabilized cells were washed with PBS and DNA was stained using 0.02 mg/ml propidium iodide (Sigma-Aldrich; Merck KGaA) and 0.2 mg/ml RNaseA (Qiagen, Inc., Valencia, CA, USA) in PBS/0.1% Triton X-100 (Sigma-Aldrich; Merck KGaA) for 30 min at room temperature in the dark. The cell cycle was analyzed with a BD-LSRFORTESSA flow cytometer (BD Biosciences; Becton, Dickinson and Company, Franklin Lakes, NJ, USA) and Flowing software 2.5.1 (www.floving-software.com/).

Immunofluorescence staining. A total of 7.5×10^4 cells (all cell lines) were plated onto Lab-Tek II Chamber Slides (Thermo Fisher Scientific, Inc.) with a diameter of 18 mm and then incubated in 12-well plates overnight at 37°C prior to treatment. Following 24 h of treatment with MLN8237 or DMSO at the indicated concentrations (10 μ M for HepG2, and 1 μ M for HepT1, HUH6 and HUH7), cells were fixed in 4% formaldehyde-phosphate-buffered saline for 15 min at room temperature, permeabilized for 15 min with 0.15% Triton X-100 in PBS at room temperature and blocked for 30 min with 1% bovine serum albumin (BSA; no. 8076.1; Carl Roth GmbH + Co., KG, Karlsruhe, Germany) in PBS at room temperature. Cells were then incubated with rat-anti-human α -tubulin (cat. no. CBL270; EMD Millipore, Billerica, MA, USA) 1:100 diluted in 1% (v/v) BSA in PBS overnight at 4°C in a wet chamber. Following several washing steps with PBS, cells were permeabilized for 10 min with 0.15% Triton X-100 in PBS at room temperature and blocked for 7 min at room temperature in 1% (v/v) BSA in PBS. Cells were then incubated for 45 min in the dark with Alexa Fluor 555 Goat anti-rat IgG (H+L) (Life technologies, Carlsbad, CA, USA) at a dilution of 1:200. After three rinses with PBS, microscope slides were mounted with Vectashield containing 4,6-diamidino-2-phenylindole (DAPI) (Vector Laboratories Inc., Burlingame, CA, USA). Images were acquired using the Olympus FluoView™ FV1000 confocal microscope.

Bisulfite pyrosequencing. The methylation status of 3 CpG-rich regions at the *MYCN/MYCNOS* locus was determined via bisulfite pyrosequencing. Briefly, the genomic DNA of 30 HB and 11 normal liver tissues was bisulfite modified using an Epitect Bisulfite kit (Qiagen, Inc.) according to the manufacturer's instructions. Subsequent PCR amplification was performed using the following forward (F) and reverse (R)

pyrosequencing primers (PS) designed with PyroMark Assay Design software (Qiagen, Inc.): PS1-F, biotin-GGTGTGTTA-GATTTTTTAGTTAAT and PS1-R, ACAACCCCTACT CCTTACCT; PS3-F, GAGAGTTAGAATTTTGTAGTTAGG AATAGT and PS3-R, biotin-TCCCCCCTCCTTTTATATA-CAAATATCT; and PS4-F, AGTTTTTAATTAAGTTATTGG TAGGAGTAT and PS4-R, biotin-AAACCCCATATCCA-CAAATCC. Pyrosequencing was performed with the sequencing primers PS1-S (ATATCCTCCAATAACTAC AATCTAT), PS3-S (AATGGTAGTTTTTAAAGTT) and PS4-S (AGTTATTGGTAGGAGTATTTT), and data analysis was performed with the PyroMark Q24 system (Qiagen, Inc.) following the manufacturer's instructions.

Statistical analyses. Data were expressed as the mean \pm standard deviation, and statistical analyses were performed with the Student's unpaired or paired t-test, the Spearman's r correlation test and the Mann-Whitney-U test. Grouped analyses were performed by employing non-parametric one-way analysis of variance (ANOVA) with a Dunn's correction for multiple comparisons or two-way ANOVA with a Bonferroni post hoc test. $P < 0.05$ was considered to indicate a statistically significant difference. GraphPad Prism 6 biostatistics software (GraphPad Software, Inc., La Jolla, CA, USA) was used for all statistical analyses.

Results

MYCN is upregulated in pediatric liver tumors due to the transcriptional activity of its antisense transcript, MYCNOS. *MYCN* expression was initially measured via RT-qPCR at the mRNA level in a comprehensive tumor collection consisting of 47 primary HB, 4 TLCT, 10 pediatric HCC, 4 liver tumor cell lines and 16 non-tumorous liver samples. The results revealed a significant upregulation of *MYCN* expression in all tumor samples and cell lines, when compared with normal liver tissue (Fig. 1A). Notably, the marked *MYCN* upregulation gradually increased across the samples, from HCC (16.2-fold) to TLCT (57.3-fold) and finally to HB (87.4-fold). In addition, histological (Fig. 1D) and immunohistochemical staining for *MYCN* protein (Fig. 1E) in HB tissues demonstrated that *MYCN* overexpression originated from tumor cells. As pediatric liver cancers lack amplifications at the *MYCN* locus (3), the present study next investigated if the antisense transcript *MYCNOS*, which maps to the same region on the opposite strand (Fig. 2A) and has been reported to positively regulate *MYCN* transcription (18), is associated with *MYCN* overexpression. The results revealed a significant overexpression of *MYCNOS* in all tumor samples, again with highest upregulation in HB tissues (Fig. 1B). Consistent with these results, a highly significant correlation between *MYCN* and *MYCNOS* mRNA levels was detected (Fig. 1C).

In order to validate the prognostic value of this data, correlations between *MYCN* and *MYCNOS* expression and clinicopathological characteristics were evaluated. By comparing the expression levels between patients with or without clinical high risk features such as metastasis, vascular invasion, multifocal or extrahepatic growth, high PRETEXT stage, embryonal histology, and age of onset > 5 years, it was demonstrated that embryonal histology was the only

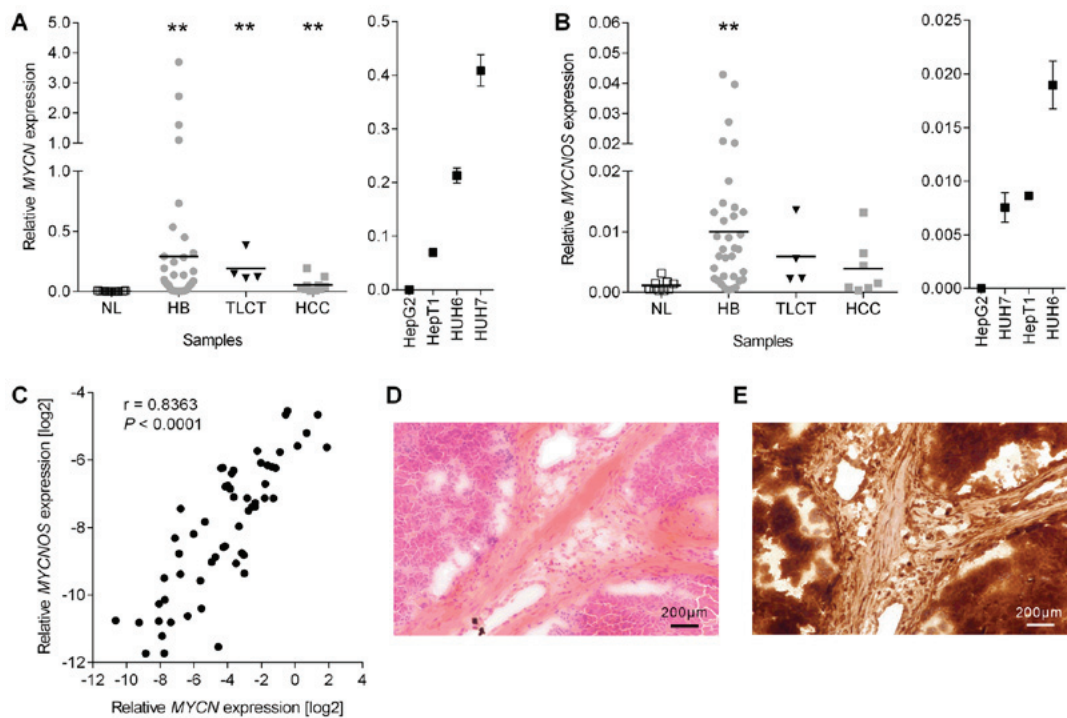


Figure 1. Expression analysis. Expression levels of (A) *MYCN* and (B) *MYCNOS* in the NL, HB, TLCT and HCC as well as the 4 liver tumor cell lines were measured by reverse transcription-quantitative polymerase chain reaction and normalized to the expression of the house-keeping gene *TBP*, with the mean presented as a horizontal line across the data points. Significances were determined by non-parametric one-way analysis of variance with a Dunn's correction for multiple comparisons. ** $P < 0.01$ vs. NL. (C) The correlation between log₂-transformed *MYCN* and *MYCNOS* expression levels was calculated using Spearman r correlation. (D and E) Representative photographs (magnification, $\times 100$; scale bars, $200\ \mu\text{m}$) of a (D) hematoxylin and eosin and (E) *MYCN* stained hepatoblastoma. NL, normal liver; HB, hepatoblastoma; TLCT, transitional liver cell tumor; HCC, hepatocellular carcinoma; *MYCN*, *MYCN* proto-oncogene basic-helix-loop-helix transcription; *MYCNOS*, *MYCN* opposite strand; *TBP*, TATA-box binding protein.

characteristic to be significantly associated with high *MYCN* and *MYCNOS* expression (Table I). There was no expression difference in regard to outcome. Collectively, these results suggest that concomitant overexpression of *MYCN* and *MYCNOS* may be a general phenomenon in pediatric liver tumors, especially in those with more undifferentiated histology.

Hypomethylation of the MYCN/MYCNOS locus is associated with high expression levels. DNA methylation has been described as an important molecular mechanism to control the transcriptional activity of genes (19). By examining 3 CpG-rich regions located at the interface of *MYCN* and *MYCNOS* (Fig. 2A) by means of pyrosequencing, the present study reported a low methylation level of $<15\%$ in all of the investigated samples (Fig. 2B-E). Notably, the median methylation level was significantly lower in the 30 pediatric liver tumors when compared with the 11 normal liver samples. Consequently, *MYCN* (Fig. 2F-H) and *MYCNOS* (data not shown) expression was negatively correlated with DNA methylation levels.

Transient MYCN knockdown impedes the growth of HB cells. Having revealed that *MYCN* was overexpressed in the vast majority of pediatric liver tumors, the present study then evaluated whether liver tumor cell growth is dependent on *MYCN*. siRNA-mediated knockdown of *MYCN* in HepT1, HUH6 and HUH7 cells (the cell lines that exhibited high *MYCN* expression levels; Fig. 1A), was therefore employed. Following transient transfection, the expression levels of

MYCN mRNA were significantly reduced after 24, 48 and 72 h when compared with the control transfected cells, being the most efficient following 24 h (Fig. 3A). The levels of *MYCNOS* expression was unchanged (data not shown). To assess whether the reduced mRNA levels of *MYCN* had an impact on cell proliferation, the present study generated cell growth curves over a time course of 0, 24, 48 and 72 h for *MYCN* depleted and control cells using MTT assays. Transient knockdown of *MYCN* led to a slightly impeded growth rate in HepT1, HUH6 and HUH7 cells when compared with control transfected cells during the first 2 days (Fig. 3B). However, the cell growth rate of HepT1 and HUH6 cells recovered 72 h post-transient si*MYCN* transfection, which could be associated with the decline of *MYCN* knockdown.

MLN8237 and JQ1 impact MYCN either at the protein or RNA level. In order to sustain the anti-proliferative effect observed following siRNA-mediated *MYCN* inhibition, the present study examined the effects of MLN8237 and JQ1, 2 known *MYCN* inhibitors already pre-clinically tested in various types of cancers (18,19), on the viability of liver cancer cells. The small molecule MLN8237 is believed to disrupt the Aurora-A/*MYCN* complex, thereby promoting the degradation of the *MYCN* protein mediated by F-box and WD repeat domain containing 7 ubiquitin ligase (20). JQ1 is an inhibitor of the bromodomain and extraterminal domain family of bromodomains that displaces the bromodomain containing 4 domain from the *MYCN* promoter and thus causes a potent depletion of *MYCN* transcription (21). As anticipated,

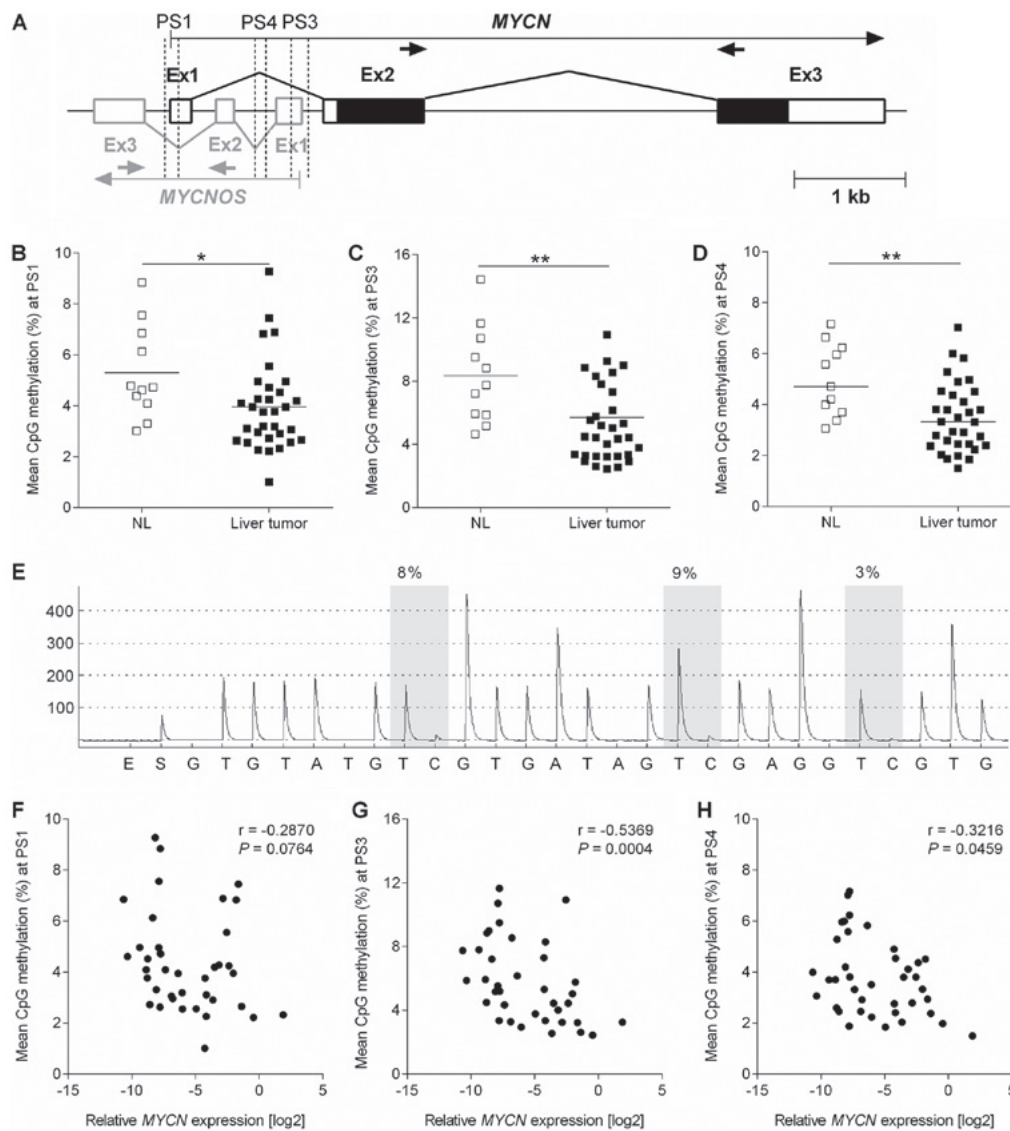


Figure 2. Methylation analysis. (A) Schematic drawing of the *MYCN/MYCNOS* locus with the exons of the *MYCN* gene (in black) and the *MYCNOS* antisense transcript (in grey); the filled boxes indicate the protein coding portions. The genomic location of the reverse transcription-quantitative polymerase chain reaction primers (arrows) and the pyrosequencing assays (dotted lines indicate the start and end of the analyzed regions) are given. (B-D) Pyrosequencing of 11 NL tissues and 30 HBs was performed to measure the percentage of DNA methylation in the CpG-rich regions for (B) PS1, (C) PS3 and (D) PS4 of the *MYCN/MYCNOS* locus. The mean methylation values (indicated by the horizontal line across the data points) and statistical significances calculated by unpaired Mann-Whitney test are presented. * $P < 0.05$ and ** $P < 0.01$, as indicated. (E) Representative pyrogram trace of a NL sample obtained following the pyrosequencing of the PS4 region of the *MYCN/MYCNOS* locus containing 3 CpG sites (with potentially methylated cytosines shaded in gray). The y-axis represents the signal intensity in arbitrary units, while the x-axis shows the dispensation order. The percentage of DNA methylation at the individual CpG positions is shown above the pyrogram. (F-H) Correlation of \log_2 -transformed *MYCN* expression levels and the mean methylation values of (F) PS1, (G) PS3 and (H) PS4 were calculated using Spearman's r correlation. NL, normal liver; HB, hepatoblastoma; *MYCN*, *MYCN* proto-oncogene basic-helix-loop-helix transcription; *MYCNOS*, *MYCN* opposite strand; PS1-4, pyrosequencing primers 1-4.

MLN8237 treatment resulted in a marked reduction in *MYCN* protein levels in the 3 tumor cell lines with high *MYCN* expression, namely HepT1, HUH6 and HUH7 (Fig. 4A). Notably, a concomitant reduction in *MYCN* transcripts was also observed in HepT1 and HUH7 cells, for which there is currently no explanation at the molecular level. By contrast, the major effect of JQ1 treatment was the downregulation of *MYCN* mRNA observed in all tumor cell lines, which resulted in reduced protein levels in the three cell lines that highly expressed *MYCN* (Fig. 4B). The low *MYCN* expressing cell line, HepG2 (Fig. 1A), exhibited unchanged protein levels upon treatment with JQ1 and MLN8237 (Fig. 4A and B). In conclusion, MLN8237 and JQ1 are potent *MYCN* inhibitors

that interfere with *MYCN* protein abundance via different molecular mechanisms.

MLN8237 and JQ1 induce dose-dependent growth arrest by trapping cells in either the G1/G0 or G2 phase. To investigate the role of *MYCN* inhibition as a possible treatment option in pediatric liver tumors, the present study examined the effect of MLN8237 and JQ1 on the viability of 4 liver cancer cell lines using MTT assays. Treatment with MLN8237 resulted in a potent reduction of cell viability in a dose-dependent manner in the 3 cell lines with high *MYCN* expression, whereas the *MYCN* low expressing cell line HepG2 was unaffected by the treatment (Fig. 5A). Similarly, treatment with low doses

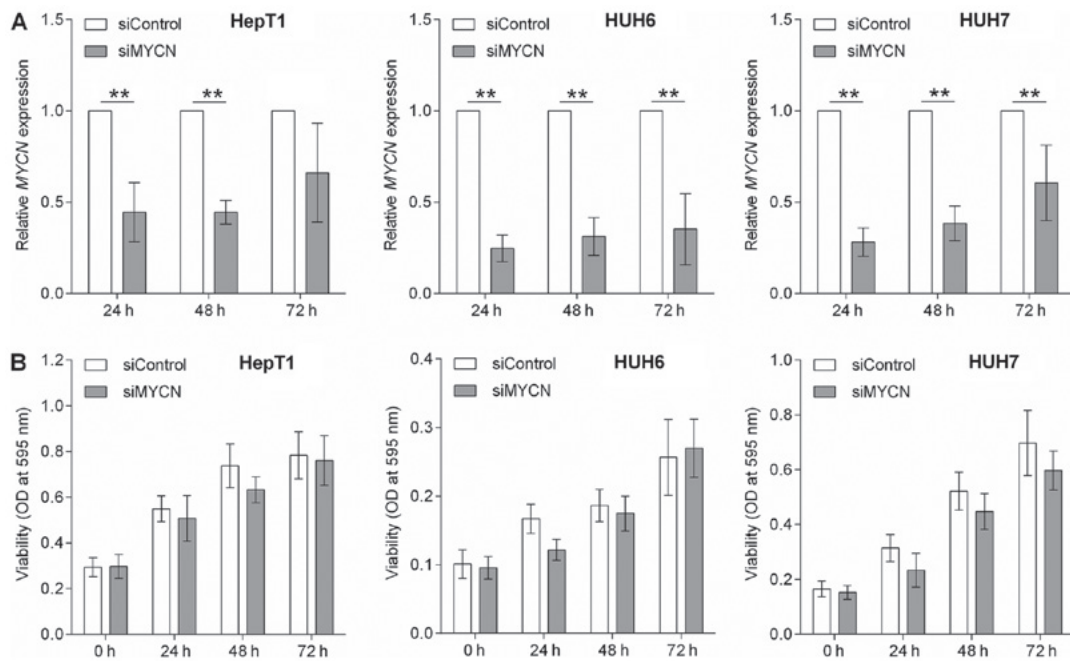


Figure 3. *MYCN* knockdown. (A) HepT1, HUH6 and HUH7 cells were transiently transfected with either siRNA against *MYCN* (siMYCN) or non-targeting control siRNA (siControl), and the mRNA expression of *MYCN* was determined by reverse transcription-quantitative polymerase chain reaction at 24, 48 and 72 h post-transfection and normalized to the house-keeping gene *TBP*. Data are presented as the mean \pm standard deviation of 4 biological replicates and were standardized to the siControl. Statistical significances were calculated using the paired Student t-test. ** $P < 0.01$, as indicated. (B) The cell viability of siMYCN or siControl transiently transfected HepT1, HUH6 and HUH7 cells was assessed at the indicated time points using MTT assays and OD measurements. The values are presented as the mean of 6 biological replicates \pm standard deviation. *MYCN*, MYCN proto-oncogene basic-helix-loop-helix transcription; *MYCNOS*, MYCN opposite strand; siRNA/si-, small interfering RNA; *TBP*, TATA-box binding protein; OD, optical density.

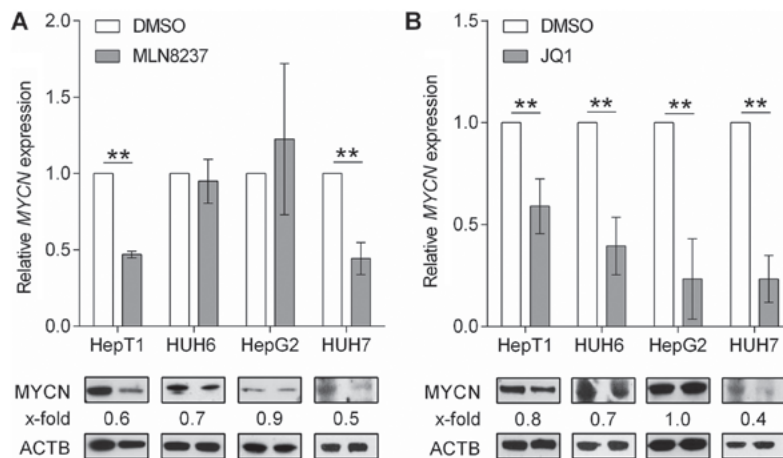


Figure 4. *MYCN* inhibition. Analysis of *MYCN*/*MYCN* mRNA and protein levels at 48 h post-treatment with vehicle (DMSO) and the *MYCN* inhibitors, (A) MLN8237 (10 μ M for HepG2, and 1.0 μ M for HepT1, HUH6, and HUH7) and (B) JQ1 (10 μ M for HepT1 and HepG2, and 0.5 μ M for HUH6 and HUH7) using reverse transcription-quantitative polymerase chain reaction and western blotting, respectively. The expression of *MYCN* was normalized to the mRNA levels of the house-keeping gene *TBP* and is presented as fold changes to the DMSO control. Data are presented as the mean \pm standard deviation of 3 biological replicates. ** $P < 0.01$, as indicated. Quantification of the *MYCN* protein (67 kDa) was performed via densitometry, with the fold reduction compared with the house-keeping protein ACTB (45 kDa) displayed on top of each band. The treated and untreated samples of each cell line were always run on the same blot and simultaneously probed with *MYCN* and ACTB antibodies. ACTB signals were detected with an exposure time of 5 sec, *MYCN* of 6 min (HUH7, HepT1 and HUH6) and 15 min (HepG2) due to their varying protein levels in the respective cell lines. *MYCN*, MYCN proto-oncogene basic-helix-loop-helix transcription; *MYCNOS*, MYCN opposite strand; ACTB, β -actin; DMSO, dimethyl sulfoxide; *TBP*, TATA-box binding protein.

of JQ1 led to significant reductions in the viability of HUH6 and HUH7 cells (Fig. 5B). Higher doses of 10 μ M JQ1 were required to induce a response in HepT1 and HepG2 cells (Fig. 5B). In addition, marked morphological changes were also noted following treatment with MLN8237 and JQ1, as evidenced by enlarged, rounded and swollen cells or detached and shrunken cells, respectively (Fig. 5C).

In order to analyze the cause of these morphological changes in more detail, the present study performed flow cytometry-based cell cycle analyses. MLN8237 treatment resulted in high levels of G2/M arrest and aneuploidy in all cell lines, while the fraction of cells in the G1/G0 and S phases were significantly reduced (Fig. 5D). Notably, all liver tumor cell lines exhibited an increase in the subG1 peak, which is

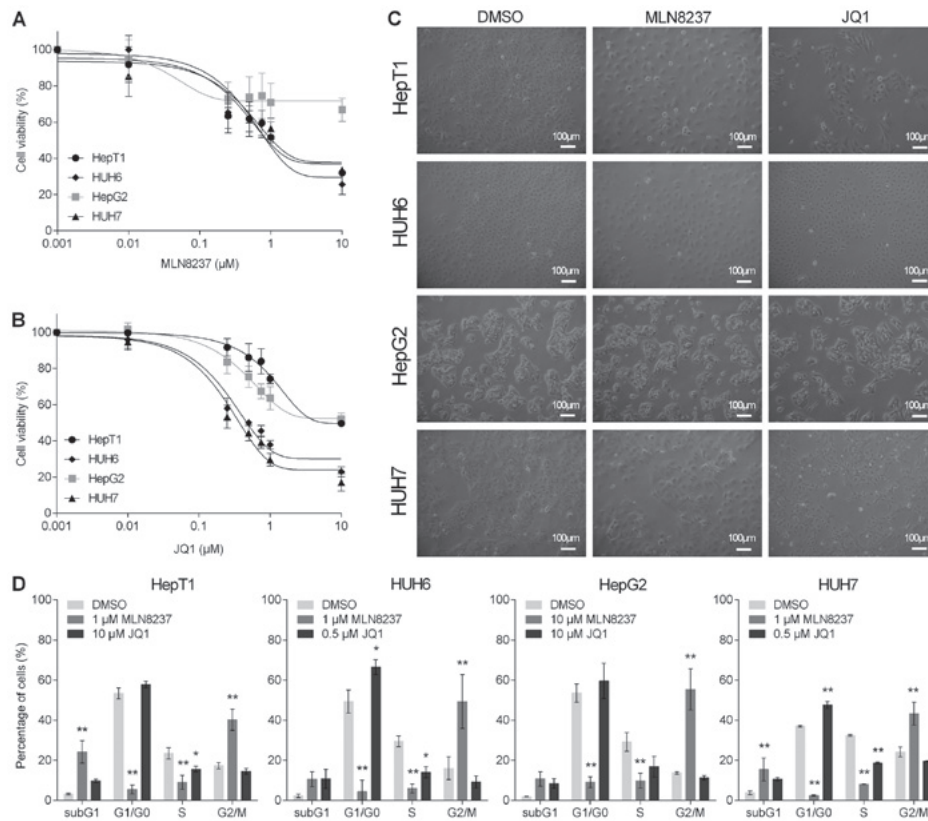


Figure 5. *MYCN* inhibition impairs cell growth. The cell viability of the hepatoblastoma cell lines (HepT1, HUH6, HepG2) and a hepatocellular carcinoma cell line (HUH7) was evaluated by MTT assay following 48 h of treatment with different concentrations (0.001, 0.01, 0.25, 0.5, 0.75, 1.0 and 10.0 μ M) of (A) MLN8237 or (B) JQ1. Values are presented as the mean \pm standard deviation of 5 independent experiments performed in duplicates. (C) Morphological changes in the cell lines following 48 h of treatment with vehicle (DMSO) and MLN8237 (10 μ M for HepG2, and 1.0 μ M for HepT1, HUH6 and HUH7) or JQ1 (10 μ M for HepT1 and HepG2, and 0.5 μ M for HUH6 and HUH7) was detected by microscopy (magnification, x100; scale bars, 100 μ m). (D) Flow cytometric analysis of cell cycle phases of propidium iodide-stained liver tumor cells in response to 48 h of treatment with vehicle (DMSO) and MLN8237 or JQ1 (concentrations as aforementioned). Data are presented as the mean \pm standard deviation of 3 biological replicates. Statistical significances from the two-way analysis of variance and the Bonferroni post hoc test are presented. * $P < 0.05$ and ** $P < 0.01$ vs. DMSO. *MYCN*, *MYC* proto-oncogene basic-helix-loop-helix transcription; DMSO, dimethyl sulfoxide.

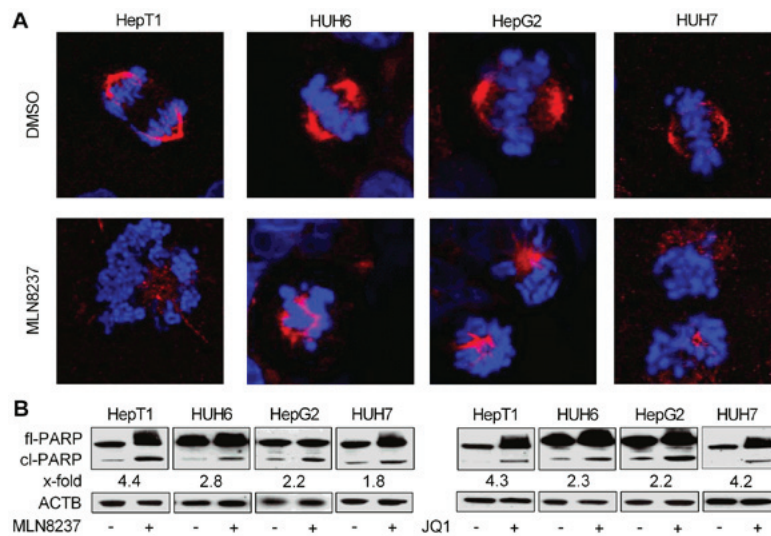


Figure 6. *MYCN* inhibition induces apoptosis. (A) Immunofluorescent staining of the spindles of liver tumor cells treated for 24 h with DMSO or MLN8237 (10 μ M for HepG2, and 1.0 μ M for HepT1, HUH6 and HUH7) using an antibody against α -tubulin (depicted in red). DNA was counterstained with DAPI (depicted in blue). Magnification, x400. (B) Immunoblots presenting the levels of fl-PARP protein (116 kDa), cl-PARP (89 kDa), and the house-keeping protein ACTB (45 kDa) at 48 h following the addition of DMSO, MLN8237 or JQ1 (10 μ M for HepT1 and HepG2, and 0.5 μ M for HUH6 and HUH7). The numbers below each of the PARP bands indicates the fold induction of cl-PARP normalized to ACTB. Treated and untreated samples of each cell line were always run on the same blot and simultaneously probed with PARP and ACTB antibodies. ACTB signals were detected with an exposure time of 5 sec, and for PARP 30 sec (HepT1 and HUH7) and 5 min (HUH6 and HepG2) due to their varying protein levels in the respective cell lines. *MYCN*, *MYC* proto-oncogene basic-helix-loop-helix transcription; DMSO, dimethyl sulfoxide; PARP, poly(adenosine diphosphate-ribose) polymerase; fl-, full-length; cl-, cleaved; ACTB, β -actin.

indicative of apoptotic events. In JQ1-treated cells, a strong induction of apoptosis was observed in all cell lines, as indicated by the prominent subG1 peak. In addition, significant G1/G0 arrest was detected in the HUH6 and HUH7 cells that were highly sensitive to JQ1 treatment in the viability assays (Fig. 5D). In conclusion, the MYCN inhibitors MLN8237 and JQ1 reduced cell viability and changed the morphology of liver cancer cell lines by arresting cells either in the G1/G0 or G2 phase.

MLN8237 and JQ1 cause spindle disturbances and/or apoptosis. As treatment with MLN8237, but not JQ1, led to cellular swelling and marked G2/M arrest, and is known to induce spindle pole abnormalities (22), the present study wanted to analyze if this may be due to disruption of the mitotic spindle apparatus. Using immunofluorescent staining of α -tubulin and confocal microscopy, discontinuous spindles and missegregated chromosomes in MLN8237-treated cells were observed, whereas control cells displayed a proper spindle apparatus and nicely ordered chromosomes in metaphase (Fig. 6A).

As flow cytometric analysis of MLN8237- and JQ1-treated cells showed a marked induction of apoptosis as evidenced by the fragmented DNA in the subG1 peak, the present study wanted to further corroborate this finding via a qualitative apoptosis assay. Western blot analysis revealed high levels of proteolytically cleaved PARP, a known downstream event elicited by caspase-induced apoptosis, following MYCN inhibition by MLN8237 and JQ1. This result confirms the assumption that the two MYCN inhibitors exert their anti-proliferative capabilities at least in part through apoptosis (Fig. 6B).

Discussion

Molecular profiling of HB serves an important role in stratifying patients into different risk groups (4). Due to the strikingly low mutation rate, molecular stratification of HB is largely determined by gene expression rather than genetic events (3). While the 16-gene HB classifier is already able to divide patients into 2 distinct risk groups based on gene expression signatures, additional biomarkers are required to predict the efficacy of targeted therapeutics (10). The present study revealed that *MYCN* and *MYCNOS* expression was significantly upregulated in HB. Furthermore, *MYCN* expression appeared to be a positive predictive marker for the response to MYCN inhibition, since HB cells with high *MYCN* expression were more susceptible to MLN8237 and JQ1 treatment. Therefore, *MYCN* and *MYCNOS* might be useful biomarkers for patients with HB in predicting their response to treatment with MYCN inhibitors.

It is the patients in the high-risk group who would particularly benefit from a more targeted therapy approach, as they are normally treated with a combination of cisplatin and doxorubicin (23). These two chemotherapeutic agents cause common immediate side effects and doxorubicin in particular has severe late effects including cardiomyopathy, congestive heart failure and the development of secondary malignancies that can arise years after the treatment has been completed (24,25). Previous studies on other solid types of

cancer have shown promising synergies when combining a cisplatin-backbone with either JQ1 or MLN8237 (26,27). It seems reasonable that HB patients with *MYCN* overexpressing tumors might also benefit from a combined regimen of cisplatin and a MYCN inhibitor, thereby reducing overall chemotherapy doses and preventing the subsequent effects from the more toxic and untargeted agents such as doxorubicin.

While *MYC* is the most common deregulated protooncogene in human cancers, *MYCN* deregulation is rare and seems to serve a specific role in pediatric malignancies (28,29). *MYCN* expression is strictly controlled during embryonal development and the activation of *MYCN* expression can be observed in a variety of pediatric tumors including neuroblastoma, medulloblastoma, rhabdomyosarcoma and gliomas (30). Activation of *MYCN* in these tumors is generally caused by amplification or alterations in other oncogenes that are able to enhance the expression of *MYCN* or stabilize its protein. *MYCNOS* has been shown to positively regulate *MYCN* expression in rhabdomyosarcoma and neuroblastoma harbouring *MYCN*-amplifications (31). Although *MYCN* is not amplified in HB, the present results suggest that *MYCNOS* may be an important driver of *MYCN* overexpression in HB.

Notably, a recent study reported that *MYCN* was able to directly bind the promoter region of *Lin-28* homolog B (*LIN28B*) and activate its transcription in neuroblastoma. In fact, *MYCN* expression exhibited a strong positive correlation to *LIN28B* expression in primary neuroblastoma (32). Another previous study demonstrated that elevated *LIN28B* expression in neuroblastoma was in turn capable of interfering with the let-7 mediated repression of *MYCN* (33). *LIN28B* is able to sequester let-7, leading to elevated *MYCN* expression and neuroblastoma formation in mice (31). *LIN28B* is also a known driver of HB as well as other liver-associated malignancies and its overexpression was shown to be sufficient for HB initiation and maintenance in mice (34). Notably, the present study detected a strong correlation between *LIN28B* and *MYCN* expression in primary HB tissues (data not shown), which is suggestive of an additional mechanism to trigger *MYCN* overexpression, similar to the mechanisms observed in neuroblastoma.

In conclusion, the results of the present study suggest that *MYCN* overexpression may be a common feature of pediatric liver malignancies, comprising HB, TLCT and HCC. While there seem to be various mechanisms through which *MYCN* overexpression arises, *MYCN* itself appears to be a promising biomarker for HB. Targeting *MYCN* with small molecules such as MLN8237 and JQ1 may help to improve outcomes and reduce the long-term effects of conventional chemotherapy protocols in patients with HB. However, preclinical testing of the therapeutic efficacy of these inhibitors in patient-derived HB xenograft models (35) is an absolute necessity.

Acknowledgements

The authors would like to acknowledge the assistance of Ms. Fatemeh Promoli and Ms. Marion Bertow for their technical support, Dr. Rebecca Maxwell for critically reviewing the manuscript and Professor Torsten Pietsch (Institute of Neuropathology, University of Bonn, Bonn, Germany) for supplying the HepT1 cell line.

Funding

The present study was supported by the Bettina Bräu Foundation (Munich, Germany) and the Gänseblümchen Foundation (Voerde, Germany).

Availability of data and materials

The datasets used and/or analyzed during the current study are available from the corresponding author on reasonable request.

Authors' contributions

CE designed experiments, acquired, analyzed and interpreted the data, and wrote the manuscript. AB interpreted the data and wrote the manuscript. CV analyzed the histopathology results and provided the samples. KB and BH contributed and analyzed the clinical data and gave scientific advice. DvS provided the samples, contributed and analyzed clinical data and critically reviewed the manuscript for important intellectual content. RK conceived the study, obtained funding, designed the experiments, analyzed and interpreted the data, wrote the manuscript, and directed the overall research. All authors discussed the results and implications, and reviewed and approved the final manuscript.

Ethics approval and consent to participate

Written informed consent was obtained from each patient and the study protocol was approved by the Ethics Committee of Ludwig-Maximilian-University (Munich, Germany; no. 431-11).

Patient consent for publication

Not applicable.

Competing interests

The authors declare that they have no competing interests.

References

- Mann JR, Kasthuri N, Raafat F, Pincott JR, Parkes SE, Muir KR, Ingram LC and Cameron AH: Malignant hepatic tumours in children: Incidence, clinical features and aetiology. *Paediatr Perinat Epidemiol* 4: 276-289, 1990.
- Zimmermann A: The emerging family of hepatoblastoma tumours: From ontogenesis to oncogenesis. *Eur J Cancer* 41: 1503-1514, 2005.
- Eichenmüller M, Trippel F, Kreuder M, Beck A, Schwarzmayr T, Häberle B, Cairo S, Leuschner I, von Schweinitz D, Strom TM, *et al*: The genomic landscape of hepatoblastoma and their progenies with HCC-like features. *J Hepatol* 61: 1312-1320, 2014.
- Sumazin P, Chen Y, Treviño LR, Sarabia SF, Hampton OA, Patel K, Mistretta TA, Zorman B, Thompson P, Heczey A, *et al*: Genomic analysis of hepatoblastoma identifies distinct molecular and prognostic subgroups. *Hepatology* 65: 104-121, 2017.
- de La Coste A, Romagnolo B, Billuart P, Renard CA, Buendia MA, Soubbrane O, Fabre M, Chelly J, Beldjord C, Kahn A, *et al*: Somatic mutations of the beta-catenin gene are frequent in mouse and human hepatocellular carcinomas. *Proc Natl Acad Sci USA* 95: 8847-8851, 1998.
- Taniguchi K, Roberts LR, Aderca IN, Dong X, Qian C, Murphy LM, Nagorney DM, Burgart LJ, Roche PC, Smith DI, *et al*: Mutational spectrum of beta-catenin, AXIN1, and AXIN2 in hepatocellular carcinomas and hepatoblastomas. *Oncogene* 21: 4863-4871, 2002.
- Mokkappati S, Niopek K, Huang L, Cunniff KJ, Ruteshouser EC, deCaestecker M, Finegold MJ and Huff V: β -catenin activation in a novel liver progenitor cell type is sufficient to cause hepatocellular carcinoma and hepatoblastoma. *Cancer Res* 74: 4515-4525, 2014.
- Buendia MA: Unravelling the genetics of hepatoblastoma: Few mutations, what else? *J Hepatol* 61: 1202-1204, 2014.
- Klijn C, Durinck S, Stawiski EW, Haverty PM, Jiang Z, Liu H, Degenhardt J, Mayba O, Gnad F, Liu J, *et al*: A comprehensive transcriptional portrait of human cancer cell lines. *Nat Biotechnol* 33: 306-312, 2015.
- Cairo S, Armengol C, De Reyniès A, Wei Y, Thomas E, Renard CA, Goga A, Balakrishnan A, Semeraro M, Gresh L, *et al*: Hepatic stem-like phenotype and interplay of Wnt/beta-catenin and Myc signaling in aggressive childhood liver cancer. *Cancer Cell* 14: 471-484, 2008.
- Weber RG, Pietsch T, von Schweinitz D and Lichter P: Characterization of genomic alterations in hepatoblastomas. A role for gains on chromosomes 8q and 20 as predictors of poor outcome. *Am J Pathol* 157: 571-578, 2000.
- Vita M and Henriksson M: The Myc oncoprotein as a therapeutic target for human cancer. *Semin Cancer Biol* 16: 318-330, 2006.
- Schwab M, Westermann F, Hero B and Berthold F: Neuroblastoma: Biology and molecular and chromosomal pathology. *Lancet Oncol* 4: 472-480, 2003.
- Kretzner L, Blackwood EM and Eisenman RN: Transcriptional activities of the Myc and Max proteins in mammalian cells. *Curr Top Microbiol Immunol* 182: 435-443, 1992.
- Kress TR, Sabò A and Amati B: MYC: Connecting selective transcriptional control to global RNA production. *Nat Rev Cancer* 15: 593-607, 2015.
- Eichenmüller M, Gruner I, Hagl B, Häberle B, Müller-Höcker J, von Schweinitz D and Kappler R: Blocking the hedgehog pathway inhibits hepatoblastoma growth. *Hepatology* 49: 482-490, 2009.
- Livak KJ and Schmittgen TD: Analysis of relative gene expression data using real-time quantitative PCR and the 2⁻(Delta Delta C(T)) method. *Methods* 25: 402-408, 2001.
- Vadie N, Saayman S, Lenox A, Ackley A, Clemson M, Burdach J, Hart J, Vogt PK and Morris KV: MYCNOS functions as an antisense RNA regulating MYCN. *RNA Biol* 12: 893-899, 2015.
- Baylin SB and Ohm JE: Epigenetic gene silencing in cancer - a mechanism for early oncogenic pathway addiction? *Nat Rev Cancer* 6: 107-116, 2006.
- Brockmann M, Poon E, Berry T, Carstensen A, Deubzer HE, Rycak L, Jamin Y, Thway K, Robinson SP, Roels F, *et al*: Small molecule inhibitors of aurora-a induce proteasomal degradation of N-myc in childhood neuroblastoma. *Cancer Cell* 24: 75-89, 2013.
- Schnepp RW and Maris JM: Targeting MYCN: A good BET for improving neuroblastoma therapy? *Cancer Discov* 3: 255-257, 2013.
- Asteriti IA, Giubettini M, Lavia P and Guarguaglini G: Aurora-A inactivation causes mitotic spindle pole fragmentation by unbalancing microtubule-generated forces. *Mol Cancer* 10: 131, 2011.
- Hiyama E: Pediatric hepatoblastoma: Diagnosis and treatment. *Transl Pediatr* 3: 293-299, 2014.
- Sivaprakasam P, Gupta AA, Greenberg ML, Capra M and Nathan PC: Survival and long-term outcomes in children with hepatoblastoma treated with continuous infusion of cisplatin and doxorubicin. *J Pediatr Hematol Oncol* 33: e226-e230, 2011.
- Lipshultz SE, Sambatakos P, Maguire M, Karnik R, Ross SW, Franco VI and Miller TL: Cardiotoxicity and cardioprotection in childhood cancer. *Acta Haematol* 132: 391-399, 2014.
- Sehdev V, Peng D, Soutto M, Washington MK, Revetta F, Ecsedy J, Zaika A, Rau TT, Schneider-Stock R, Belkhir A, *et al*: The aurora kinase A inhibitor MLN8237 enhances cisplatin-induced cell death in esophageal adenocarcinoma cells. *Mol Cancer Ther* 11: 763-774, 2012.
- Zanellato I, Colangelo D and Osella D: JQ1, a BET inhibitor, synergizes with cisplatin and induces apoptosis in highly chemoresistant malignant pleural mesothelioma cells. *Curr Cancer Drug Targets* 18: 816-828, 2018.
- Kalkat M, De Melo J, Hickman KA, Lourenco C, Redel C, Reseta D, Tamachi A, Tu WB and Penn LZ: MYC Deregulation in Primary Human Cancers. *Genes (Basel)* 8: 8, 2017.
- Sala A: Editorial: Targeting MYCN in Pediatric Cancers. *Front Oncol* 4: 330, 2015.

30. Rickman DS, Schulte JH and Eilers M: The Expanding World of N-MYC-Driven Tumors. *Cancer Discov* 8: 150-163, 2018.
31. O'Brien EM, Selfe JL, Martins AS, Walters ZS and Shipley JM: The long non-coding RNA MYCNOS-01 regulates MYCN protein levels and affects growth of MYCN-amplified rhabdomyosarcoma and neuroblastoma cells. *BMC Cancer* 18: 217, 2018.
32. Beckers A, Van Peer G, Carter DR, Gartlgruber M, Herrmann C, Agarwal S, Helmoortel HH, Althoff K, Molenaar JJ, Cheung BB, *et al*: MYCN-driven regulatory mechanisms controlling LIN28B in neuroblastoma. *Cancer Lett* 366: 123-132, 2015.
33. Molenaar JJ, Domingo-Fernández R, Ebus ME, Lindner S, Koster J, Drabek K, Mestdagh P, van Sluis P, Valentijn LJ, van Nes J, *et al*: LIN28B induces neuroblastoma and enhances MYCN levels via let-7 suppression. *Nat Genet* 44: 1199-1206, 2012.
34. Nguyen LH, Robinton DA, Seligson MT, Wu L, Li L, Rakheja D, Comerford SA, Ramezani S, Sun X, Parikh MS, *et al*: Lin28b is sufficient to drive liver cancer and necessary for its maintenance in murine models. *Cancer Cell* 26: 248-261, 2014.
35. Nicolle D, Fabre M, Simon-Coma M, Gorse A, Kappler R, Nonell L, Mallo M, Haidar H, Déas O, Mussini C, *et al*: Patient-derived mouse xenografts from pediatric liver cancer predict tumor recurrence and advise clinical management. *Hepatology* 64: 1121-1135, 2016.